Cut	ν_e CC Efficiency	ν_μ CC Efficiency	ν_μ NC Efficiency
$Q_t > 1.0$ GeV	.673	.628	.034
$p_t < 2.5$ GeV	.965	.977	.682
$\Delta z < 15$ cm	.923	.971	.848
$Q^2 > 2$ GeV^2	.861	.848	.655
$W^2 > 5$ GeV^2	.967	.932	.828
Muon in event	.969	.047	.932
Lead Particle electron ID	.799	.007	.038
Total	.382	.00015	.00030

Table 6.4: MC Event Selection Cuts and Efficiencies on MC Samples.

of ν_μ in the MC sample was normalized to match the level in the data sample. In Table 6.6 the final number of selected events and the number expected from Monte Carlo for both ν_e and ν_μ are given.

In the end, 721 ν_e events and 52598 ν_μ events were observed. The shape of the ν_e spectrum is shown in Figure 6.22. A break down of the event population can be found in Table 6.7. The Monte Carlo prediction of 722.3 events for the number of ν_e compares well with the number found in the data. There was a 4.3% background (see Figure 6.23) in the ν_e's and negligible background in the ν_μ's. Note the low statistics in the ν_e background; it was small but not negligible.

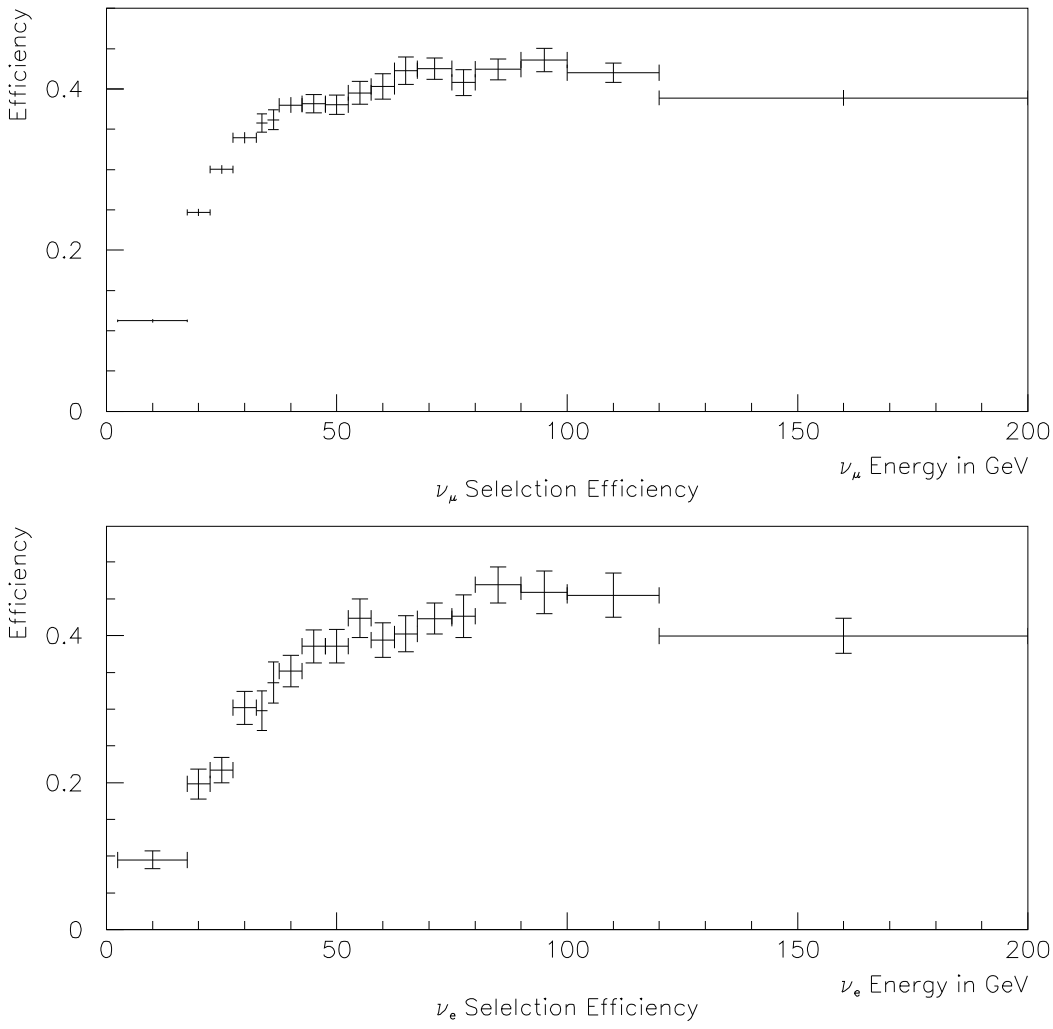

Figure 6.21: Selection Efficiencies for ν_μ and ν_e versus Energy.

Cut	ν_μ CC Efficiency	ν_e CC Efficiency	ν_μ NC Efficiency
$Q_t > 1.0$ GeV	.628	.673	.033
$p_t < 2.5$ GeV	.977	.966	.681
$\Delta z < 15$ cm	.971	.923	.848
$Q^2 > 2$ GeV^2	.861	.848	.655
$W^2 > 5$ GeV^2	.967	.932	.828
Lead Particle muon ID	.899	.001	.020
Total	.419	.0006	.00021

Table 6.5: MC Event Selection Cuts and Efficiencies on MC Samples.

	Selected ν_e	Selected ν_μ
ν_e CC Monte Carlo	691.1	1.1
ν_μ CC Monte Carlo	18.4	52589.9
ν_μ NC Monte Carlo	12.8	7.1
Total MC	722.3	52598.1
4 DC Module Data	130.0	7643.0
8 DC Module Data	254.0	18383.0
11 DC Module Data	337.0	26572.0
Total Data	721.0	52598.0

Table 6.6: Final ν_e and ν_μ Events Selected and Predictions from Monte Carlo.

Energy Bin	Selected ν_e	Selected ν_μ
2.5- 17.5 GeV	17.0 ± 4.1	6479.0 ± 80.5
17.5- 22.5 GeV	38.0 ± 6.1	6235.0 ± 78.9
22.5- 27.5 GeV	52.0 ± 7.2	5932.0 ± 77.0
27.5- 32.5 GeV	56.0 ± 7.5	5038.0 ± 70.9
32.5- 35.0 GeV	35.0 ± 5.9	2050.0 ± 45.3
35.0- 37.5 GeV	28.0 ± 5.2	1872.0 ± 43.3
37.5- 42.5 GeV	67.0 ± 8.1	3249.0 ± 57.0
42.5- 47.5 GeV	50.0 ± 7.1	2673.0 ± 51.7
47.5- 52.5 GeV	53.0 ± 7.3	2231.0 ± 47.2
52.5- 57.5 GeV	53.0 ± 7.3	1900.0 ± 43.6
57.5- 62.5 GeV	34.0 ± 5.8	1733.0 ± 41.6
62.5- 67.5 GeV	37.0 ± 6.1	1462.0 ± 38.2
67.5- 75.0 GeV	48.0 ± 6.9	2044.0 ± 45.2
75.0- 80.0 GeV	24.0 ± 4.9	1185.0 ± 34.4
80.0- 90.0 GeV	37.0 ± 6.1	2121.0 ± 46.1
90.0-100.0 GeV	31.0 ± 5.6	1541.0 ± 39.3
100.0-120.0 GeV	29.0 ± 5.4	2154.0 ± 46.4
120.0-200.0 GeV	32.0 ± 5.7	2699.0 ± 52.0

Table 6.7: Final ν_e and ν_μ Events Selected with Errors in Each Energy Bin.

6.6 ν_μ-ν_e Spectrum Ratio

An oscillation signal would evince itself in the form of an enhancement in the low energy part of the spectrum (for low Δm^2) or over the entire spectrum (for large Δm^2). Looking directly at the ν_e spectrum is problematic because this makes the measurement extremely sensitive to fluctuations in the predicted flux and simulation. Looking at the ratio ν_e/ν_μ helps to cancel out some of this dependence but does not completely resolve the problem as ν_e's and ν_μ's have different sources. The ratio approach also cancels out other common effects such as hadronic energy resolution and event selection biases. This analysis, therefore, looks at the ratio of the two spectra.

A non-uniform binning was used for the energy spectrum. This was done in order to maintain a sufficient level of statistical significance in each channel. The energy bins were chosen so that each channel has no fewer than than 15 ν_e events (see Table 6.7).

As can be seen from a cursory scan of Figure 6.24, the agreement between the selected sample and the prediction was quite good. Over the eighteen bins there were 10 bins with an excess of the data over the Monte Carlo and 8 bins with a deficit. The χ^2 [40] used for this data sample is

$$\chi^2 = \sum_i -2\log P(n_i|\mu_i) + 2\log P(n_i|n_i) \tag{6.3}$$

where

$$P(n|\mu) = (\mu + b)^n \frac{\exp^{-\mu+b}}{n!} \tag{6.4}$$

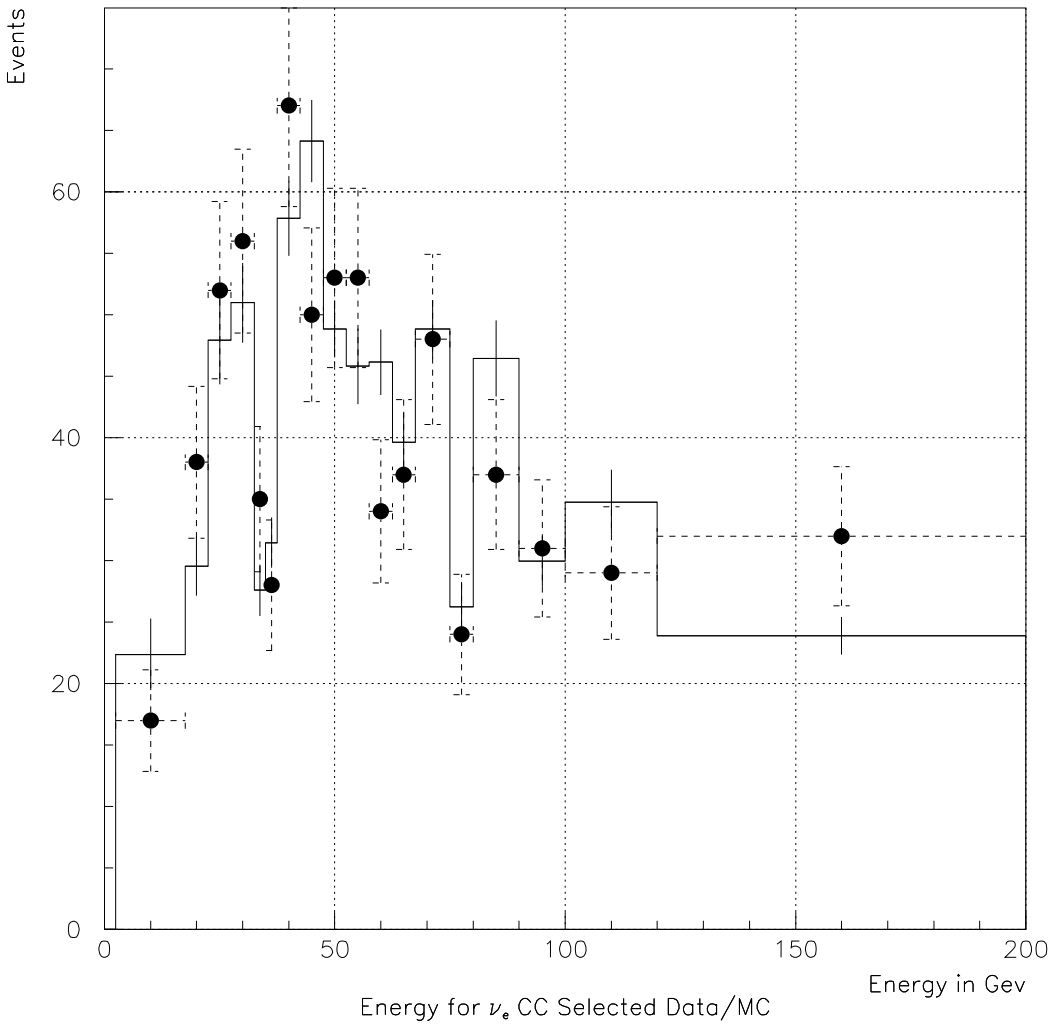

Figure 6.22: ν_e CC Selected Spectrum. The Monte Carlo is the solid line and the data are the dots.

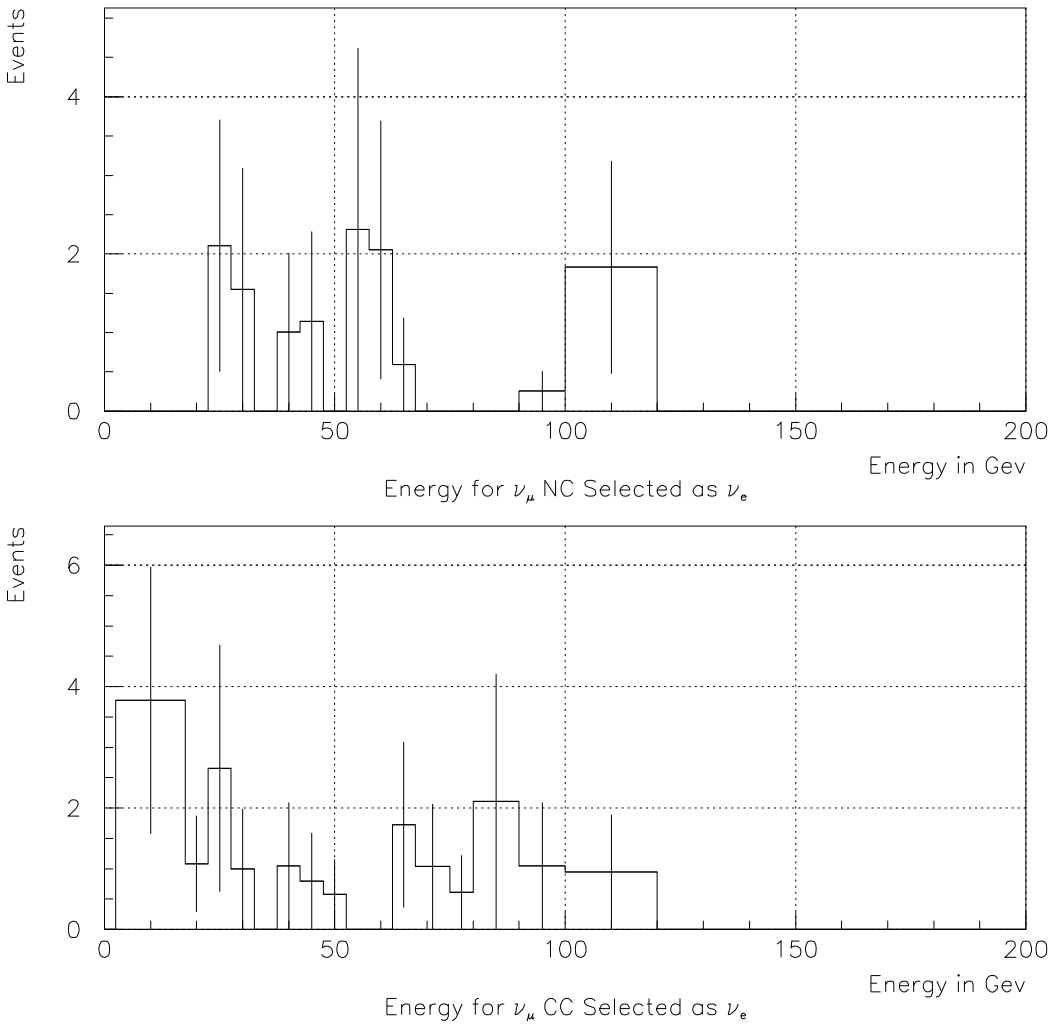

Figure 6.23: Background Shapes from ν_μ NC and CCs. The top graph is from NC and the bottom from CC.

Here μ is the number of signal events expected, b is the number of background events and n is the number of events observed.

These were summed for all energy bins and found to be 20.9 for 18 degrees of freedom. Locally, there were no regions of significant excess. It was therefore assumed that there was no excess of ν_e events over the Monte Carlo and therefore no evidence for neutrino oscillations.

The rest of the discussion will now concentrate on extracting a limit on the oscillation probability.

6.7 Setting a 90% Confidence Limit

The standard way of presenting neutrino oscillation limits is by giving a region in the plane of Δm^2 vs $\sin^2 2\theta$ for which oscillations have been ruled out at a 90% confidence level. In order to define this region, several values for Δm^2 were taken and the corresponding Monte Carlo prediction for the ratio spectrum was calculated for the $\sin^2 2\theta$ which minimizes the χ^2. Then the values of $\sin^2 2\theta$ for which the χ^2 is 2.71 over the minimum were found. For each Δm^2 there is now a value of $\sin^2 2\theta$ and these points define the 90% confidence level boundary.

6.7.1 ν_e Oscillation Contribution

The oscillation probability is a function of the energy of the incoming neutrino as well as the distance it has travelled. In order to calculate the probability

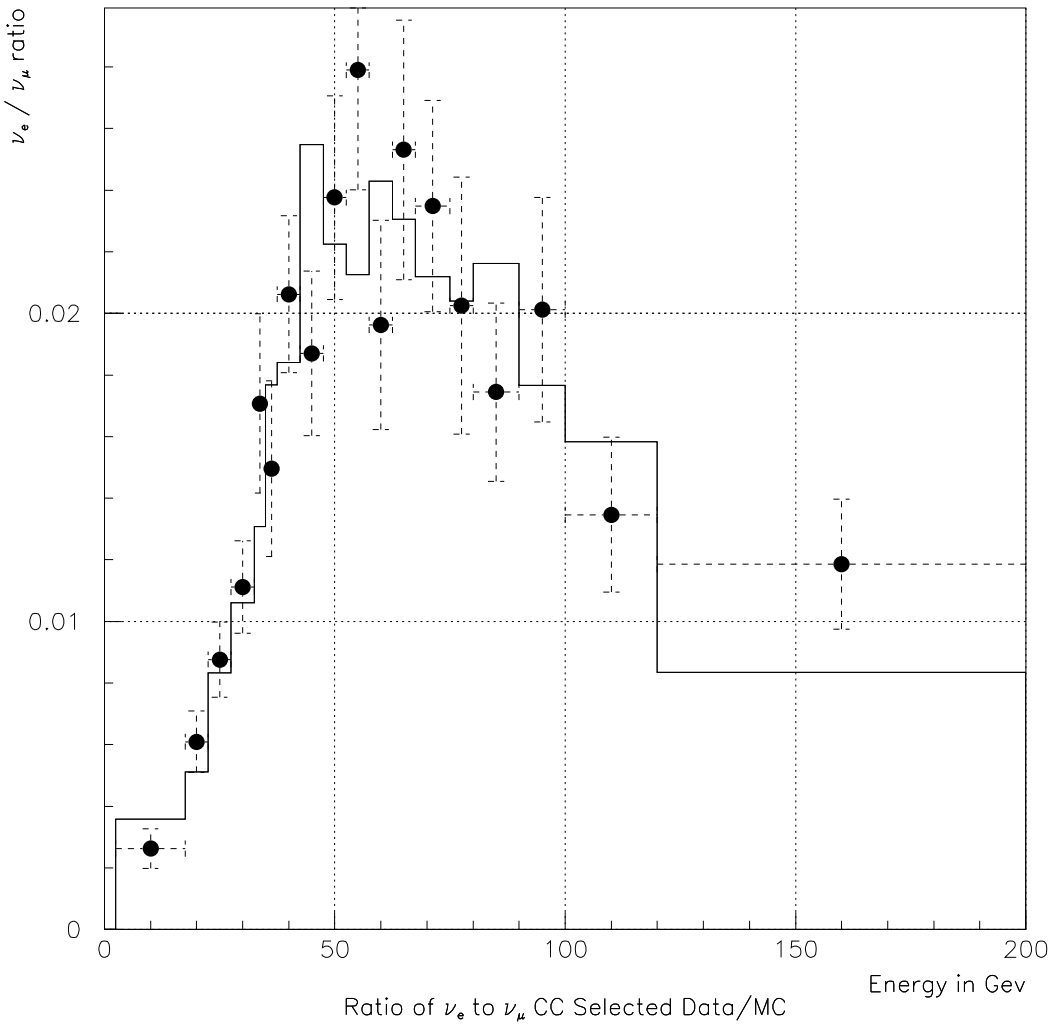

Figure 6.24: The ratio of ν_e and ν_μ CC Spectra. The solid line is Monte Carlo and the dots are the data.

$p(\nu_\mu \to \nu_e)$ that a given neutrino will oscillate, the following equation was used:

$$p(\nu_\mu \to \nu_e) = \sin^2 2\theta \sin(\frac{1.27\Delta m^2 L}{E}) \tag{6.5}$$

where E is the energy of the incoming neutrino in GeV, and L is the path length travelled in kilometers. The neutrino source is not a point source, it is in fact a 413 meter long tunnel. The oscillation probability was calculated at 200 points along the length of the tunnel and averaged. The distribution of decays along the tunnel was assumed to be flat. The difference this length effect has on the final oscillation contribution can be seen by comparing the distributions in Figure 6.25 and Figure 6.26. It can be seen that absence of corrections due to the length of the tunnel induces spikes to the spectrum which are smoothed out due to the different points of origins of neutrinos along the tunnel.

Once the oscillation probability was calculated it can be applied to the ν_μ spectrum to determine the shape of the oscillation contribution to the ν_e spectrum. This distribution is shown for four different values of Δm^2 in Figure 6.26. Then from the previous Monte Carlo study the selection efficiency and corrections from the reconstruction can be factored in to give the spectrum as it would be observed in the data. The effect is shown for four different values of Δm^2 in Figure 6.27. Finally, the oscillation contribution was added to the background ν_e spectrum from standard ν_e sources. Looking at Figure 6.28 where a contribution with a $\sin^2 2\theta$ of 0.01 has been added to the ν_e spectrum, the different effects from different Δm^2 can be seen. For low Δm^2 the excess will be seen mostly in the

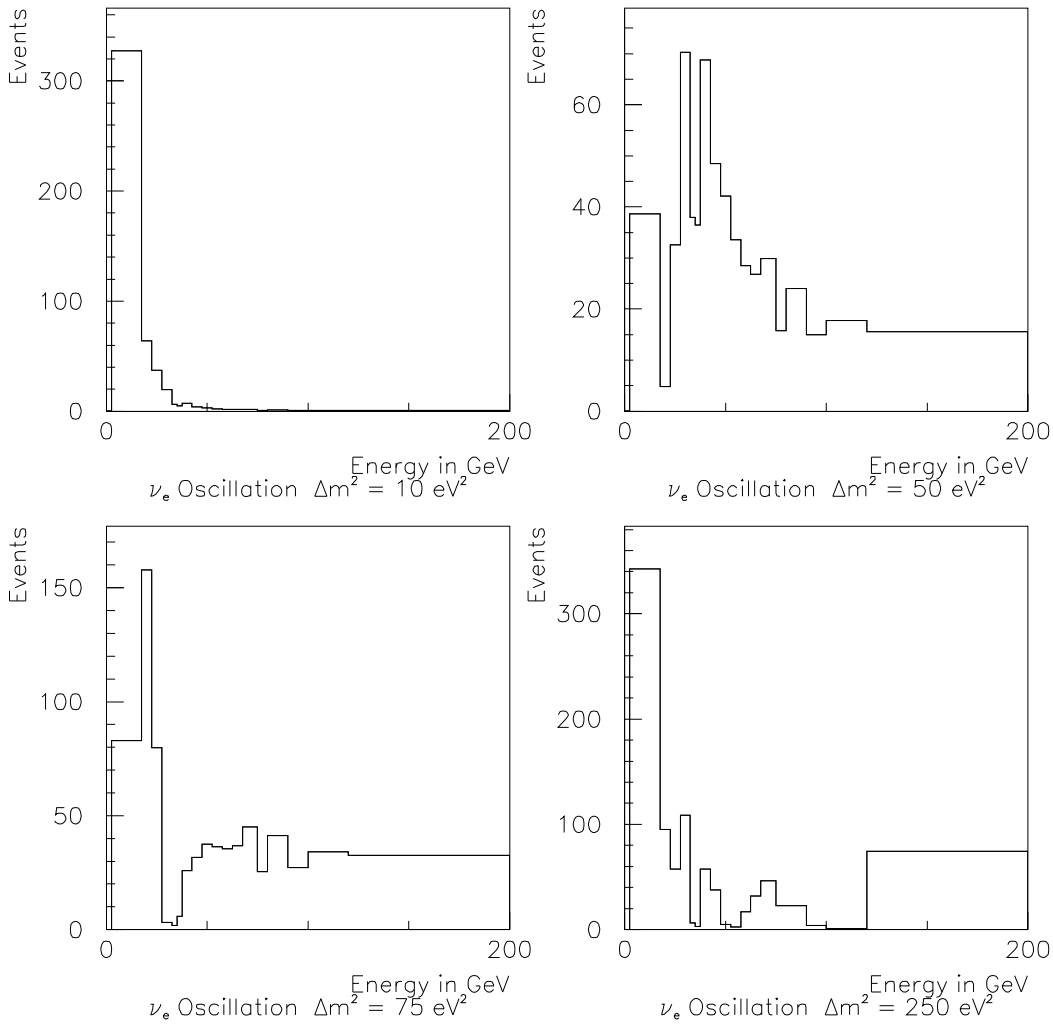

Figure 6.25: The ν_e Oscillation Contribution for Δm^2 of 10 eV$^2/c^4$, 50 eV$^2/c^4$, 100 eV$^2/c^4$, 250 eV$^2/c^4$ without the length of the tunnel taken into account.

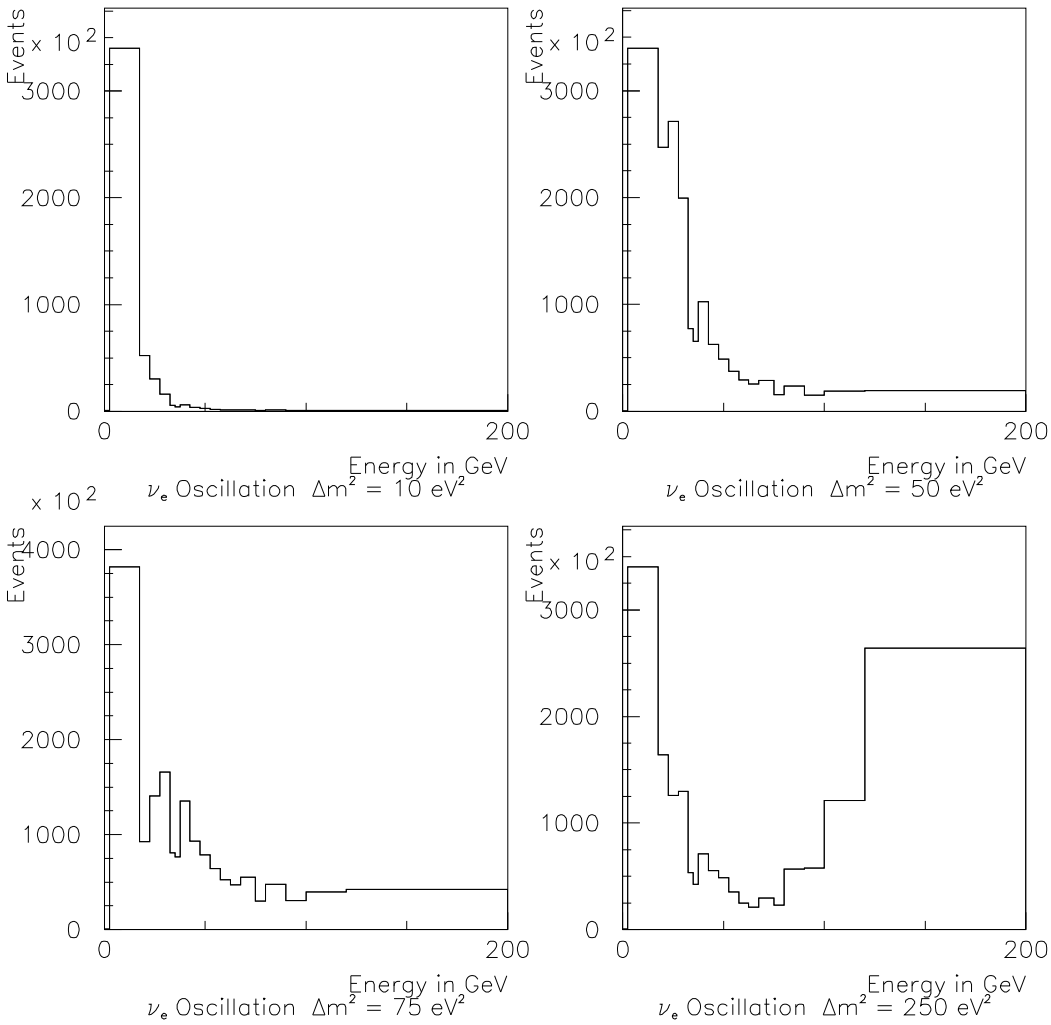

Figure 6.26: The ν_e Oscillation Contribution for Δm^2 of 10 eV$^2/c^4$, 50 eV$^2/c^4$, 100 eV$^2/c^4$, 250 eV$^2/c^4$.

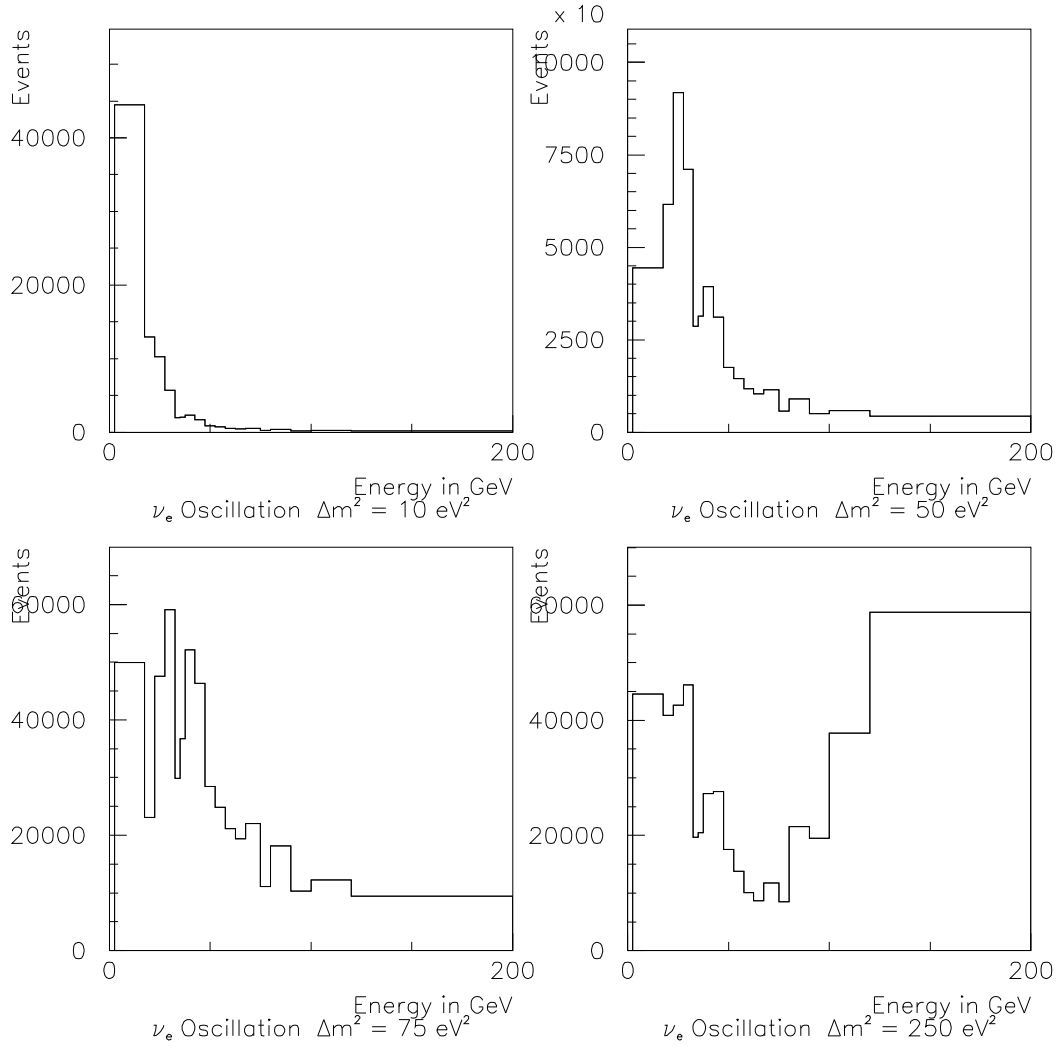

Figure 6.27: The ν_e Oscillation Contribution for Δm^2 of 10 eV$^2/c^4$, 50 eV$^2/c^4$, 100 eV$^2/c^4$, 250 eV$^2/c^4$ corrected for ν_e efficiency.

low energy region whereas, for higher Δm^2 the excess is noticeable on the whole spectrum.

6.7.2 Minimization of the χ^2

With the form of the signal available for a set of Δm^2s, it is possible to calculate the value of $\sin^2 2\theta$ that minimizes χ^2 for each value of Δm^2. For gaussian errors the standard form that χ^2 takes is:

$$\chi^2 = \sum_i \frac{(\frac{N_i^{E^{\nu_e}}(MC)+N_i^{E^{\nu_e}}(Osc)}{N_i^{E^{\nu_\mu}}(MC)} - \frac{N_i^{E^{\nu_e}}(Data)}{N_i^{E^{\nu_\mu}}(Data)})^2}{\sigma_i^2} \tag{6.6}$$

where σ_i^2 is just taken from the $\sqrt{n_i}$ where n_i is the number entries in the ith bin. This form unfortunately has the problem that for bins where the data is less than predicted the error is too small and bins where there is more data than predicted the error is too big. An alternate form for the χ^2 based on the likelihood function was used:

$$\chi^2 = 2\sum_i N_i^{E^{\nu_e}}(Predicted) - N_i^{E^{\nu_e}}(Data) + N_i^{E^{\nu_e}}(Data)\log\frac{N_i^{E^{\nu_e}}(Data)}{N_i^{E^{\nu_e}}(Predicted)} \tag{6.7}$$

where

$$N_i^{E^{\nu_e}}(Predicted) = N_i^{E^{\nu_\mu}}(Data)\frac{N_i^{E^{\nu_e}}(MC)}{N_i^{E^{\nu_\mu}}(MC)} + N_i^{E^{\nu_e}}(Osc) \tag{6.8}$$

This is derived from equations 6.3 and 6.4.

In order to find χ^2_{min} the Newton-Raphson method for finding roots was used. This method uses the the derivative of a function to extrapolate to zero and then

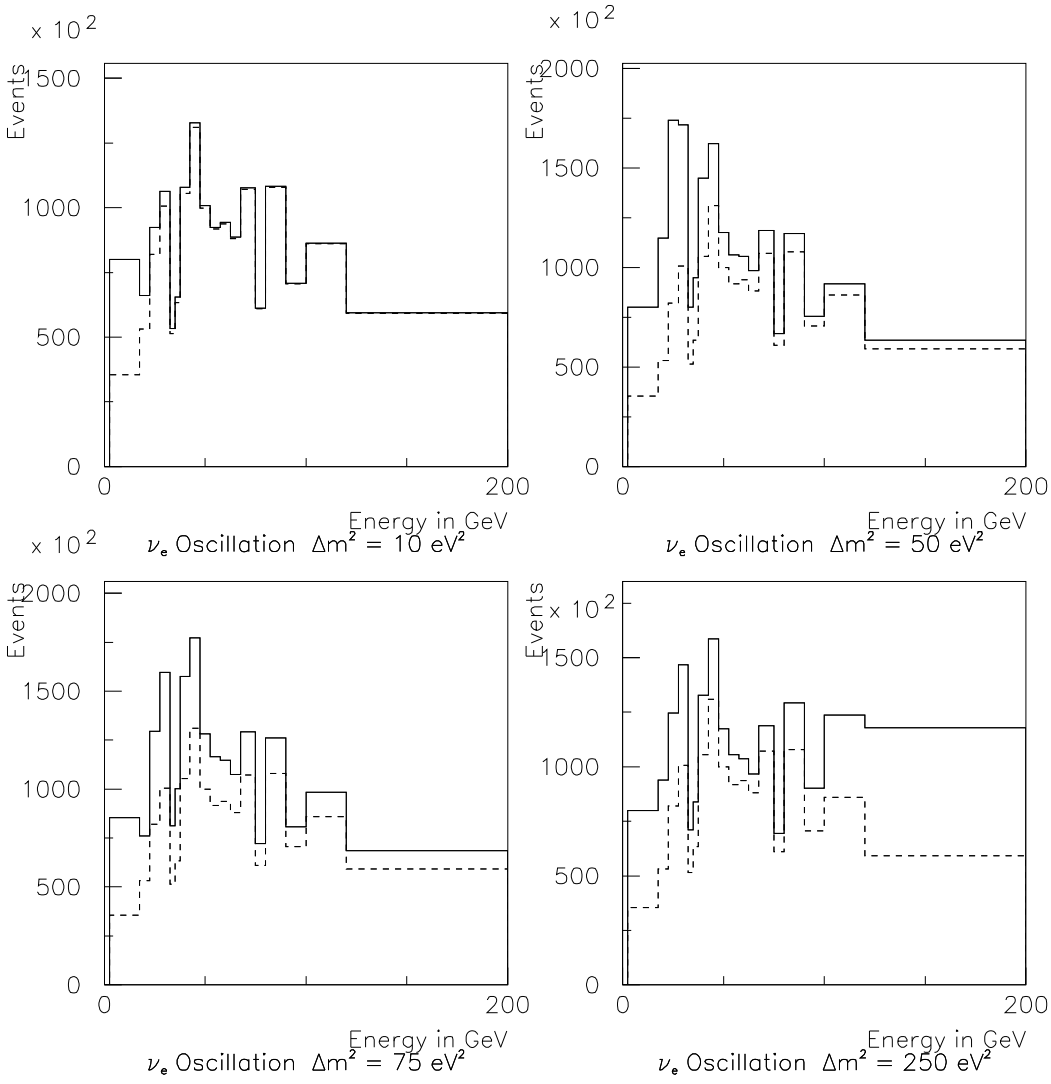

Figure 6.28: The ν_e Oscillation Contribution for Δm^2 of 10 eV$^2/c^4$, 50 eV$^2/c^4$, 100 eV$^2/c^4$, 250 eV$^2/c^4$ with $\sin^2 2\theta = 0.01$ corrected for efficiency and added to the ν_e spectrum. The dotted line is the ν_e spectrum with no oscillation contribution.

using that point as the next guess. The functional form the $N_i^{E^{\nu_e}}(Predicted)$ can be rewritten in terms of $\sin^2 2\theta$:

$$N_i^{E^{\nu_e}}(Predicted) = N_i^{E^{\nu_\mu}}(Data)\frac{N_i^{E^{\nu_e}}(MC)}{N_i^{E^{\nu_\mu}}(MC)} + \sin^2 2\theta N_i^{E^{\nu_e}}(Osc) \qquad (6.9)$$

where $N_i^{E^{\nu_e}}(Osc)$ is now the oscillation contribution for a $\sin^2 2\theta$ value of 1.

Then, taking the derivative of this function with respect to $\sin^2 2\theta$ is trivial. Minimum values of χ^2 were then sought between values of -1.0 and 10. Once a value for the minimum of χ^2 was found, then the Newton-Raphson method was used once more to find the value of $\sin^2 2\theta$ for which χ^2 is the minimum χ^2 + 2.71 which gives us the two-sided 90% confidence limit for a χ^2 distribution with one degree of freedom. This was done for for values of Δm^2 from 0.1 eV^2/c^4 up to 250 eV^2/c^4. For each of these values of Δm^2, a value of $\sin^2 2\theta$ was found. These points define the boundary of a 90% confidence level area of exclusion of neutrino oscillation in the Δm^2-$\sin^2 2\theta$ plane. It is displayed in Figure 6.29. The limit, at 250 eV^2/c^4, is 2.4×10^{-3}. Notice also the ripple in the curve with a frequency of about 20 eV^2/c^4. This is the effect of the $\sin(\frac{1.27\Delta m^2 L}{E})$ term in the oscillation probability. With an average energy of 30 GeV and the propagation distance about 1 km, a frequency of order 20 eV^2/c^4 is expected.

6.7.3 Alternative Methods

While this method is valid given that it is assumed that there was no signal in this selected data sample, there are other techniques which have historically been

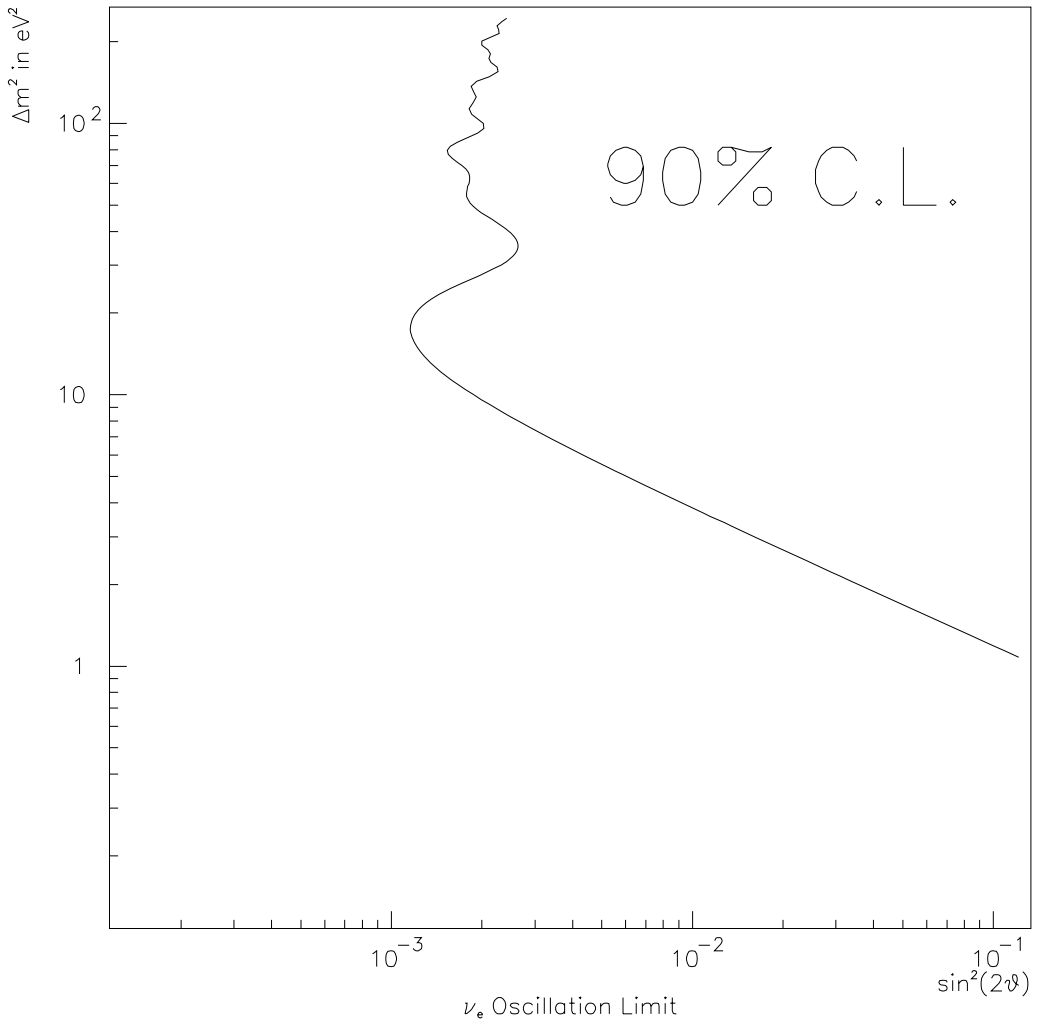

Figure 6.29: Boundary of 90% Confidence Level Exclusion of ν_e Oscillations from Statistical Errors Only.

used to perform this calculation. These methods are discussed in [41] where, also, a new method for performing this calculation is presented. These methods are referred to as the Raster Scan, the Flip-Flop Raster Scan, and the Global Scan. The method used in this analysis is called the Raster Scan.

The Flip-Flop Raster Scan makes a decision whether to set a one-sided upper limit or a two-sided interval based on what is seen in the data. If a signal with greater than three standard deviations significance is seen, then one performs the normal Raster Scan to come up with an interval of acceptance. If not an upper limit is set using the one-sided 90% C.L. $\Delta\chi^2$ value of 1.64. This method suffers from the fact that it undercovers the 90 % C.L. region.

The Global Scan makes a best fit to both Δm^2 and $\sin^2(2\theta)$, and then all points that have a χ^2 within 4.61 of this minimum value are said to be within the region of confidence. This method suffers from both under-coverage and over-coverage.

The method that was used in this analysis is not very effective at finding regions of signal if they exist. This is because it performs the limit calculation at fixed values of Δm^2. Also there is no mechanism for insuring that the limit set is meaningful (i.e., within the physical bounds). The technique proposed in [41] overcomes this flaw by using a method similar to the Global Scan, but it uses a Monte Carlo simulation to determine $\Delta\chi^2$ values for different values of Δm^2 and $\sin^2(2\theta)$ using an ordering technique proposed in the text.

6.8 Systematic Effects

Up to now only statistical errors have been taken into account, even though there are many systematic effects, including the prediction of the neutrino flux, which have not been looked at. This will now be done.

6.8.1 Modifying the Limit

The method used for modifying the limit finds errors for each effect, adds them in quadrature with each other, and then adds this sum in quadrature with the limit.

6.8.2 Kinematic Selection

This analysis is basically a counting and comparison experiment, so variations between the Monte Carlo and reality can have a strong influence on the the final result. A good way to check this is to look for systematic effects due to this selection. In order to study whether systematic effects were introduced by the selection of specific kinematic cuts, the cuts were varied and the subsequent shifts in the end results were observed.

The kinematical cuts were varied as follows.

Cut	Min	Max	Value used
Q_t	0.9 GeV	1.1 GeV	1.0 GeV
p_t	2.2 GeV	2.8 GeV	2.5 GeV
Δz	13.0 cm	17.0 cm	15.0 cm
Q^2	1.5 GeV^2	2.5 GeV^2	2.0 GeV^2
W^2	4.5 GeV^2	5.5 GeV^2	5.0 GeV^2
X and Y Vertex	120.0 cm	140.0 cm	130.0 cm

Each cut was varied individually.

The best fit value of $\sin^2(2\theta)$ was calculated for several values of the given cut in the ranges given above. A search for a systematic pattern was looked for. If none were found the error was taken to be the average shift from the original selected value for value $\sin^2(2\theta)_{BEST}$. The variation in $\sin^2(2\theta)_{BEST}$ for the different cuts can be seen in Figure 6.30 and Figure 6.31.

In Figure 6.31 it is seen that a transition between 130 and 120 cm of the vertex cut is undergone. This is near the edge of the fiducial region of NOMAD. It can be seen that this effect is of the order of about 0.3×10^{-3}, which is small compared to the statistical error. An error of 0.3×10^{-3} was assigned due to the choice of the vertex.

More significant seems to be the choice of W^2 cut. As can been seen in Figure 6.32, there is a transition region between 4 GeV^2 and 6 GeV^2. The level of this effect is of the order 0.7×10^{-3}. An error of 0.7×10^{-3} was assigned due to the choice of the W^2 cut.

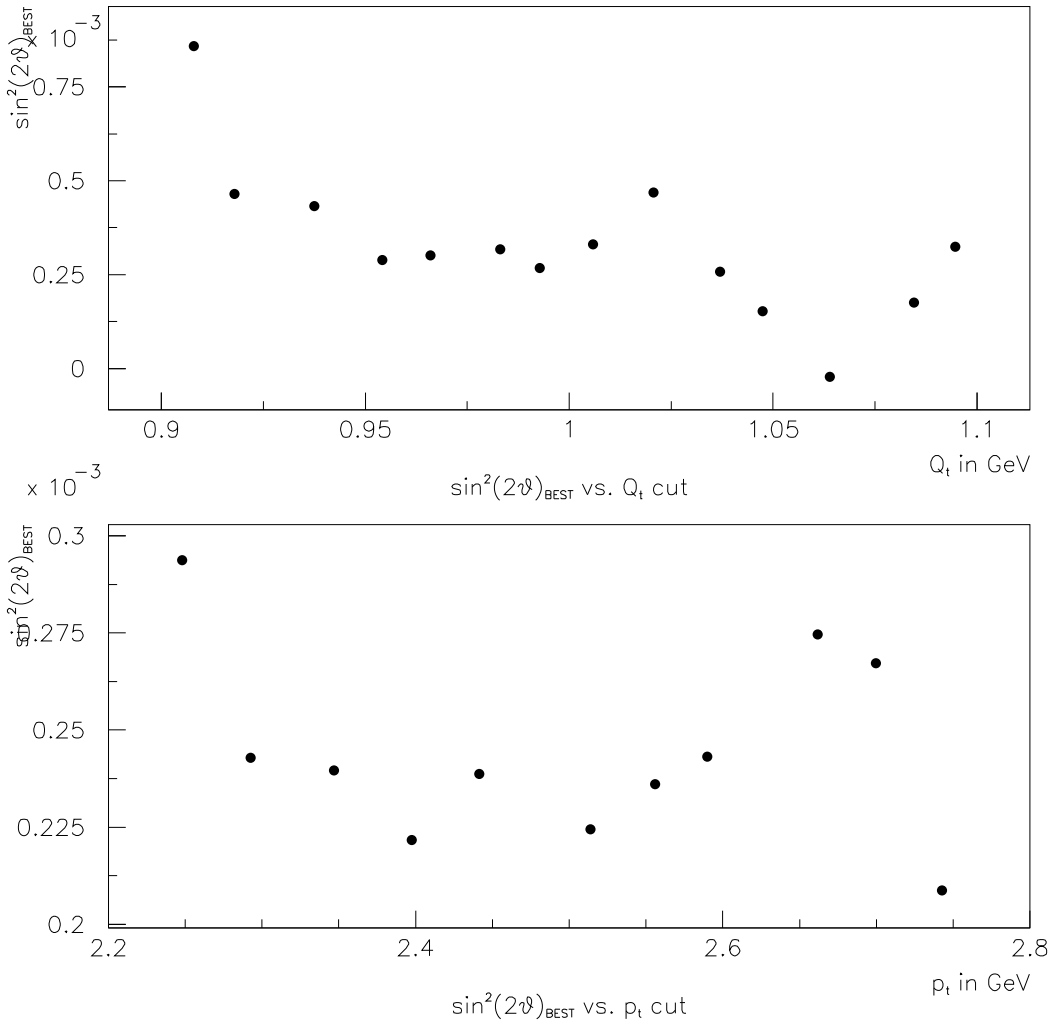

Figure 6.30: Variation in $\sin^2(2\theta)_{BEST}$ vs. Cuts on Q_t and p_t.

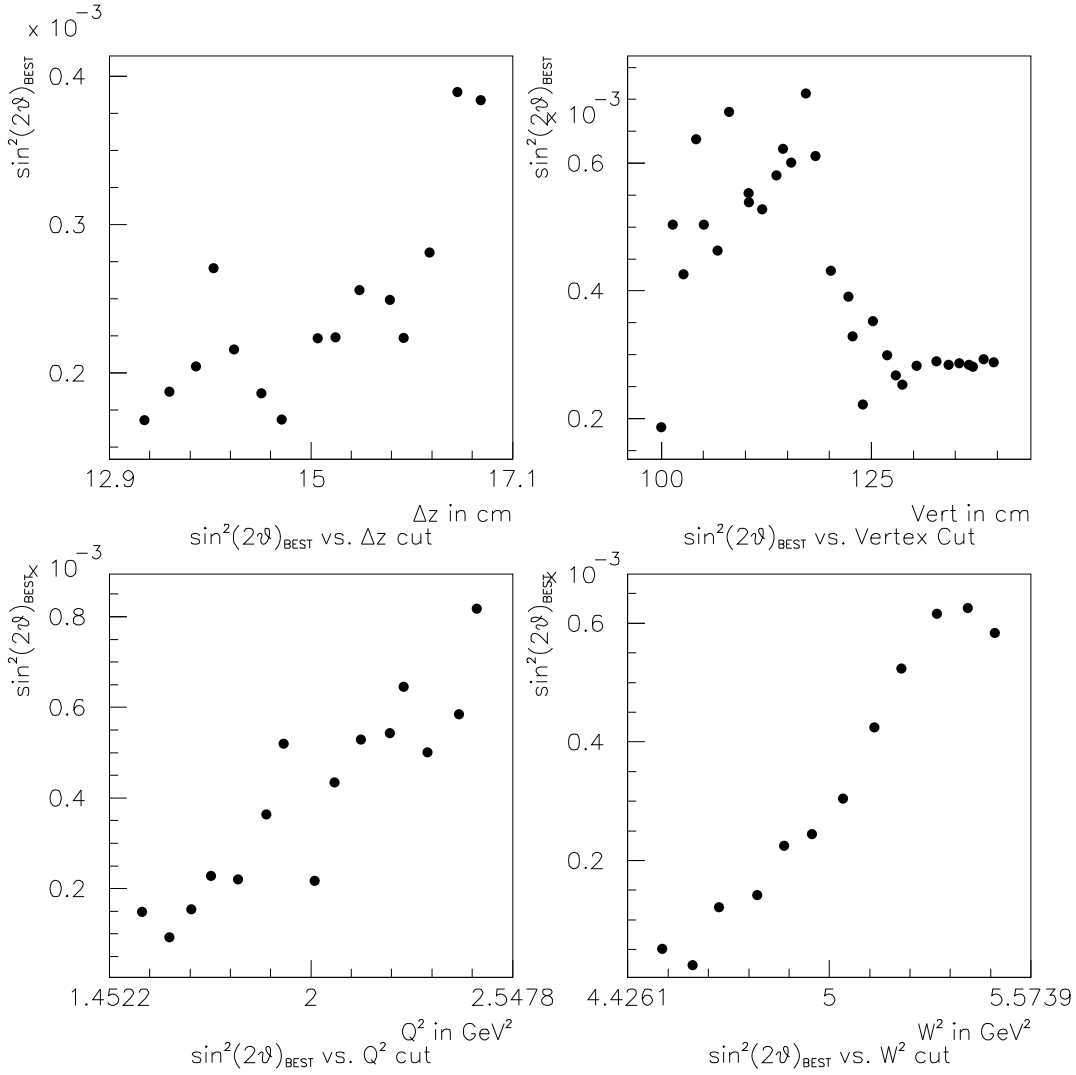

Figure 6.31: Variation in $\sin^2(2\theta)_{BEST}$ vs. Cuts on Δz, the Vertex Position, Q^2 and W^2.

A similar effect exists for the Q^2 cut (see Figure 6.32). The level of the effect is of the order of 0.5×10^{-3}. An error of 0.5×10^{-3} was assigned due to the choice of the Q^2 cut.

Trends in the other variables were not detected. The magnitude of all these effects can be see in Table 6.8.

6.8.3 Electron Selection

In order to see the effect of differences in electron selection between data and Monte Carlo, the electron selection criteria were modified and the subsequent shift in the ν_e/ν_μ ratio was looked at. The variations used were:

Cut	Min	Max	Value used
$TRDPICON$	8×10^{-3}	1.5×10^{-2}	1×10^{-2}
$E_{cal} - p_{DC}/\Delta(E_{cal} - p_{DC})$	0.0	-1.0	-0.5
$PRS_x + PRS_y$	2.0	9.0	3.0

Each criteria was varied individually.

The best fit value of $\sin^2(2\theta)$ was calculated for several values of the given cut in the ranges given above. A search for a systematic pattern was looked for. If none were found the error was taken to be the average shift from the original selected value for value $\sin^2(2\theta)_{BEST}$. The variation in $\sin^2(2\theta)_{BEST}$ can be seen in Figure 6.33.

As expected these effects are not large (see Table 6.8), as the main selection of the proper leading lepton comes from the kinematical choice of the leading

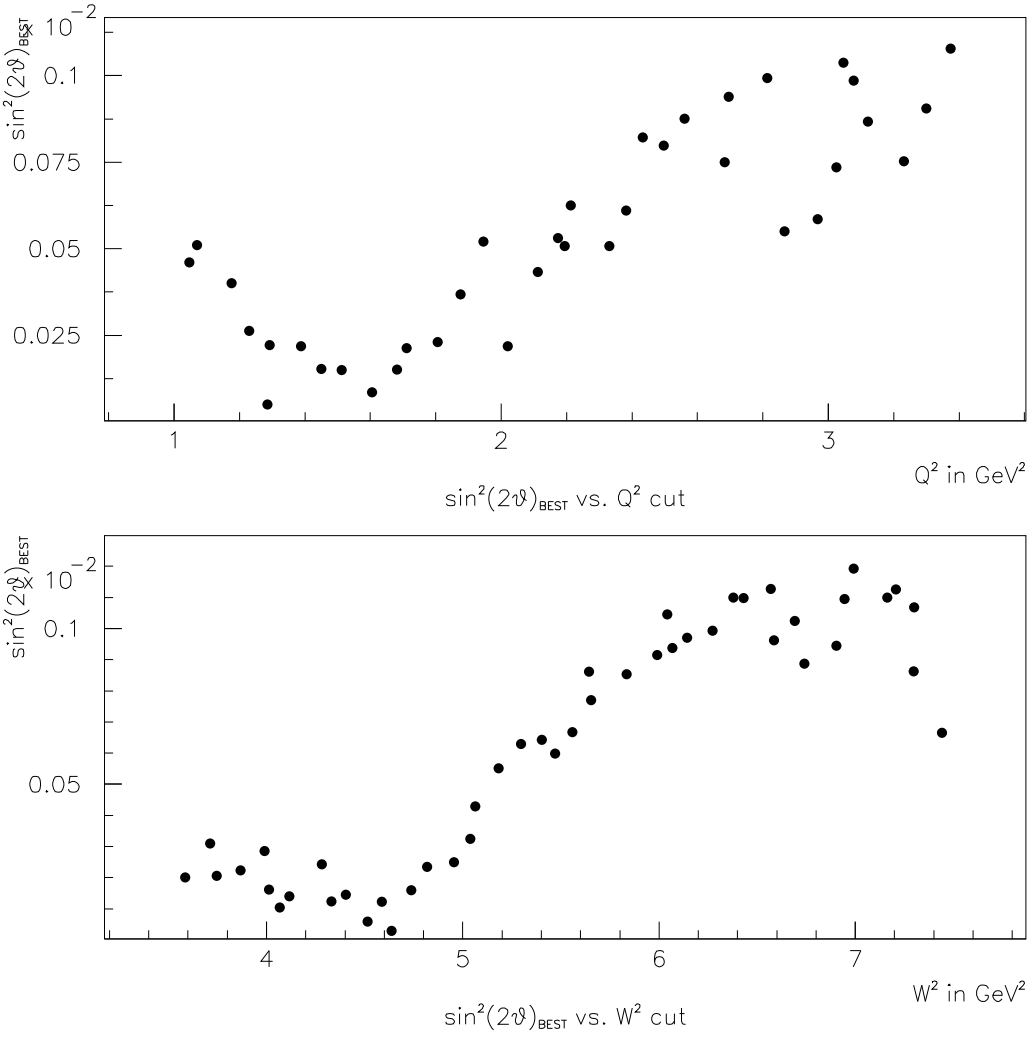

Figure 6.32: Variation in $\sin^2(2\theta)_{BEST}$ vs. Cuts on Q^2 and W^2.

lepton. Most of the error originates from the Ecal cut on $E - p/\Delta(E - p)$.

6.8.4 ν_e Flux

The error of the ν_e flux from the empirical parametrization used is 2.7% [30]. In order to see the effect on this analysis, the predicted ν_e spectrum was shifted by plus/minus this amount and the difference in the end result was observed. It can be seen that this variation is small, in Figure 6.34. In Figure 6.35 the variation can be seen to be small relative to the statistical error. The error introduced is of the order 0.9×10^{-3}. This is the single largest error.

6.8.5 Electron Track Reconstruction

The difference between muon tracks being reconstructed in the MC and data was measured to be less than 1% [35] by using tracks in the TRD. Electrons are much more difficult to measure as they scatter in the tracking media and this has not been measured very well. For this analysis we assumed an error of 3% as reasonable given the order of the effect for muons.

6.8.6 Other Effects

A study using a similar method was done by Weber [42] on the same data sample and several other systematic effects were looked at and found to be small. Among these effects were the shape of the background, the shape of the flux, event

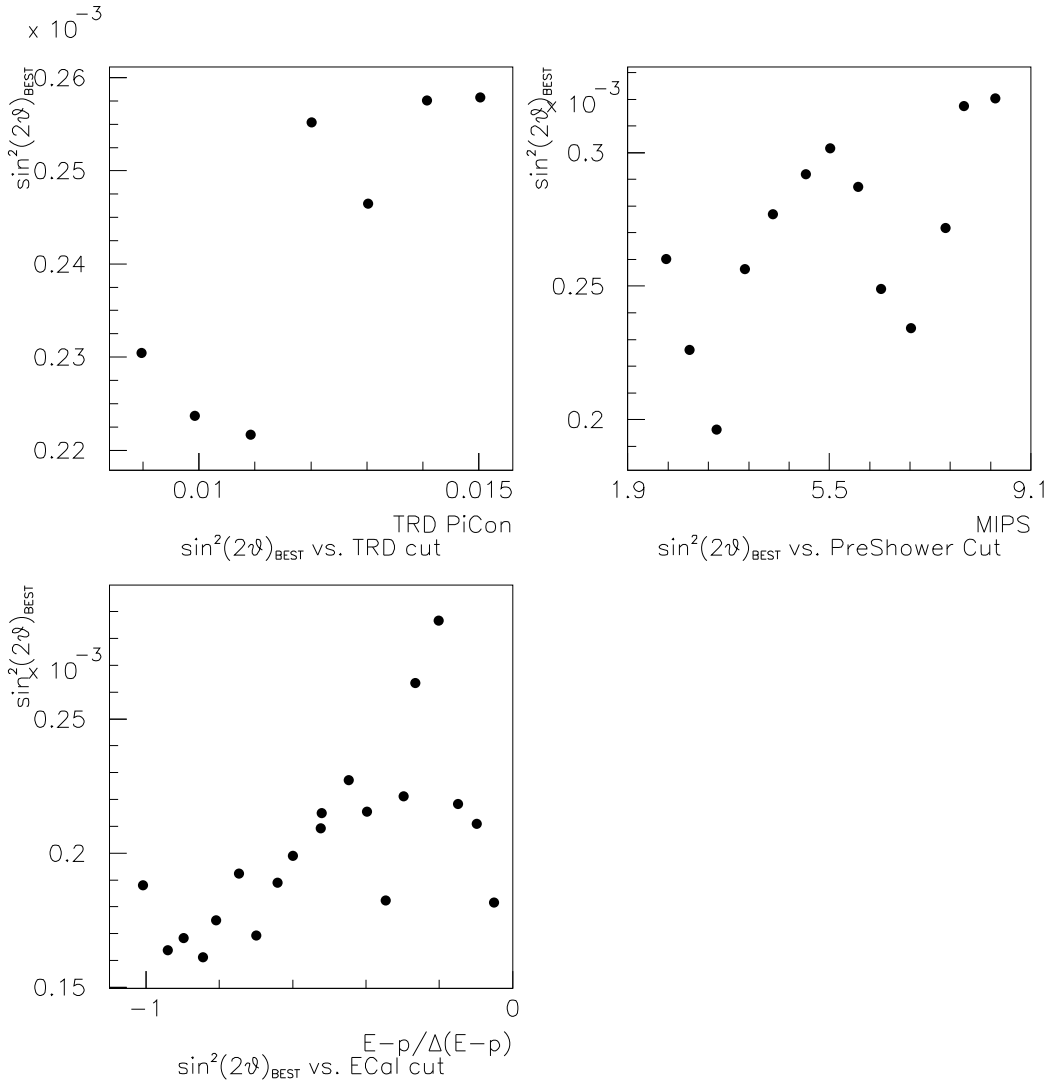

Figure 6.33: Variation in $\sin^2(2\theta)_{BEST}$ for Various Values of the Electron Selection Cuts.

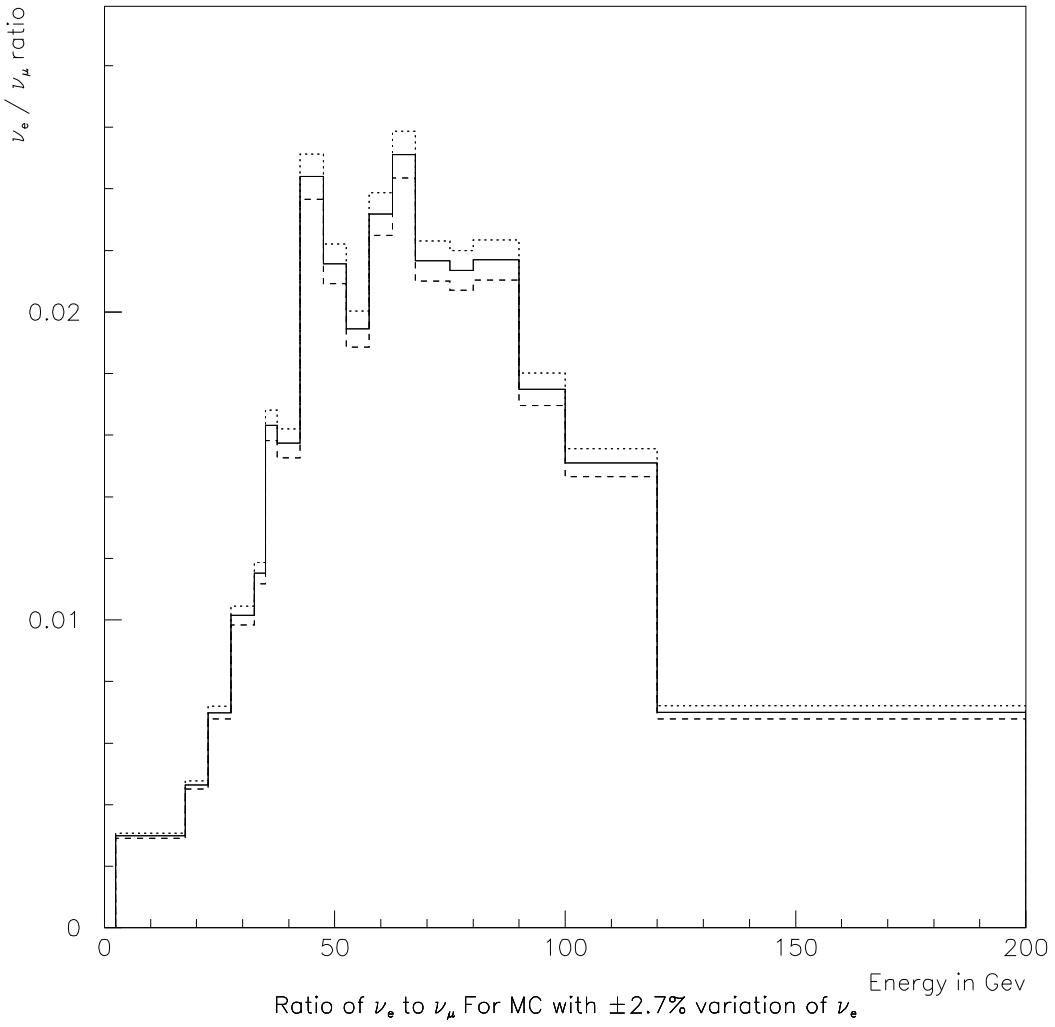

Figure 6.34: The ν_μ/ν_e Spectrum Ratio of the Simulation. The ν_e flux has been varied $\pm 2.7\%$. The solid line is the nominal ratio, the dotted line is for -2.7%, and the dashed line is for $+2.7\%$.

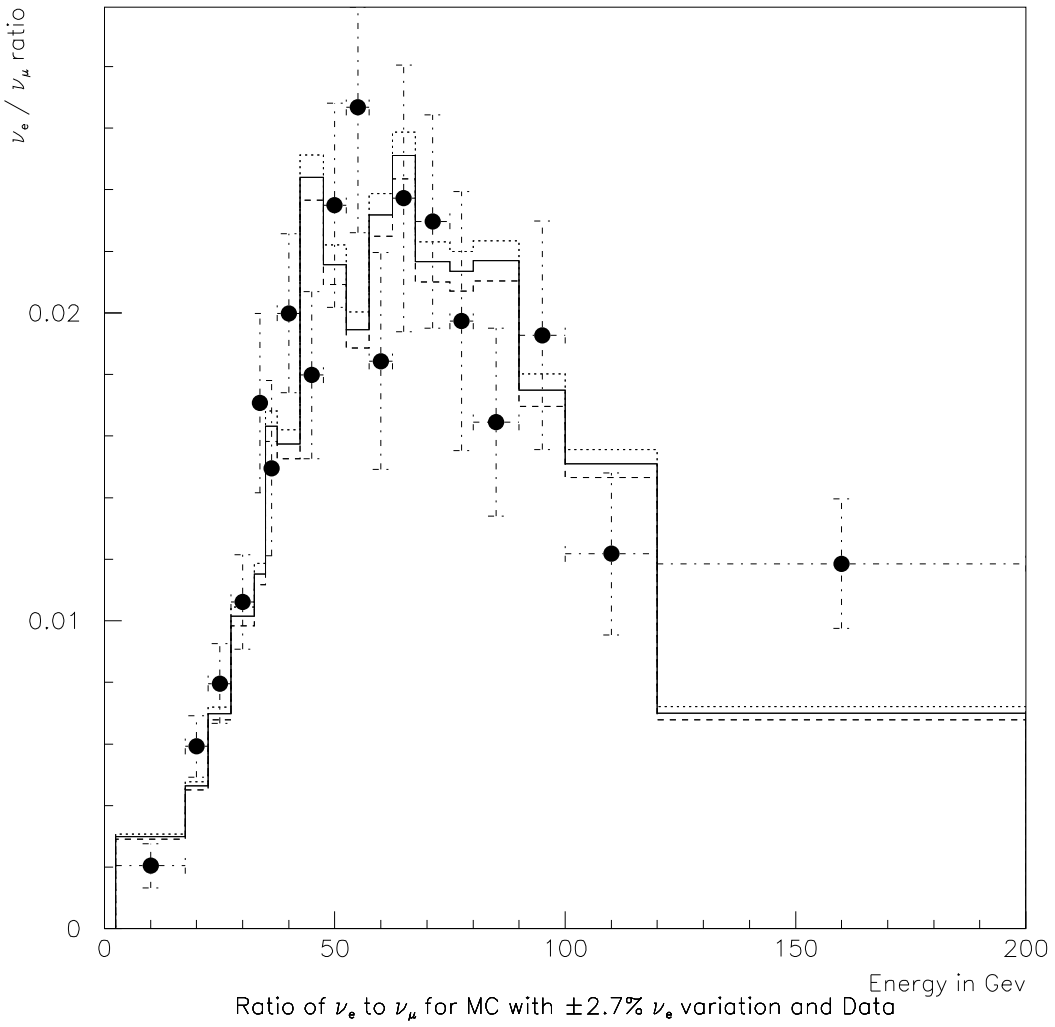

Figure 6.35: The ν_μ/ν_e Spectrum Ratio of the Simulation. The ν_e flux has been varied $\pm 2.7\%$. The solid line is the nominal ratio, the dotted line is for -2.7%, and the dashed line is for $+2.7\%$. The data, having been superimposed, is the dots.

Cut	Associated error
Q_t	0.7
p_t	0.3
Δz	0.3
Vertex	0.3
Q^2	0.5
W^2	0.7
TRD	0.04
PreShower	0.1
$E - p/\Delta(E - p)$	0.4
Flux	0.9
Electron Reconstruction	0.9

Table 6.8: Systematic Errors at the Δm Value of 250 eV^2/c^4. The errors are quoted in units of 10^{-3}.

generator cutoffs and muon identification. These effects were not taken into account in this analysis.

Chapter 7

Conclusion

A search for an excess of ν_e charged current events was conducted using the NOMAD detector with the data sample from the 1995 run in order to attempt to find a signal of excess ν_e's from the $\nu_\mu \rightarrow \nu_e$ oscillation process. A limit was then set at a 90% confidence level for this process. This is shown in Figure 7.1. The high mass limit on $\sin^2(2\theta)$ is 3.2×10^{-3}. A limit on Δm^2 is set below 1 eV^2 for full mixing and a limit of 2.1×10^{-3} can be set at the Δm^2 value of 26 eV^2 (see Table 7.1).

A large section of the LSND result in the high mass region can be excluded. This leads one to believe that if the LSND result is indeed an oscillation signal, it likely is an indication for oscillations in a lower Δm^2 region.

The major limitations of this analysis arise primarily from the limited statistical sample and the uncertainty in the beam composition. With the data samples from the 1996 and 1997 runs, the number of events should increase by close to

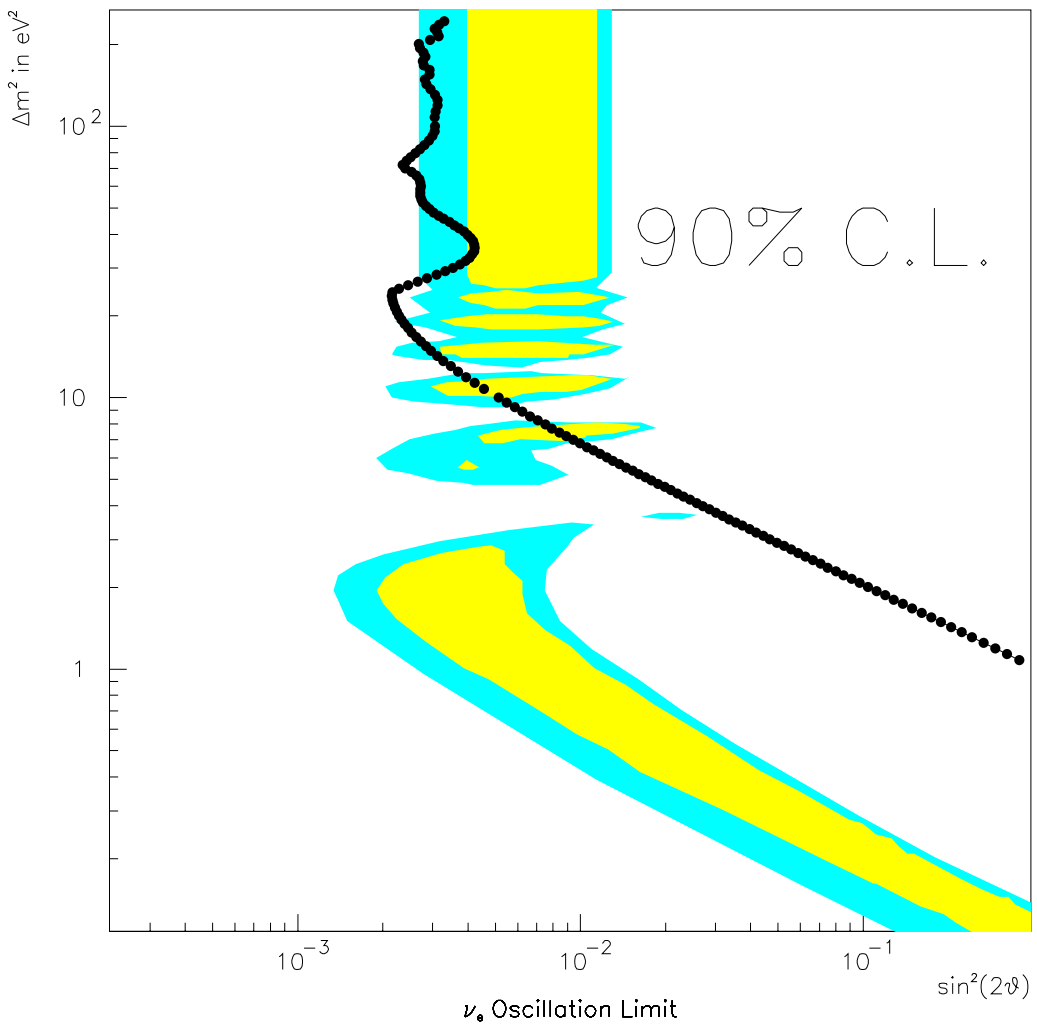

Figure 7.1: Final 90% C.L. Exclusion Region for this Analysis and the LSND Eesult. The dark line is the 90% C.L. limit for this analysis. The dark shaded region is the 99% allowed region for the LSND result and the light shaded region is the 90% allowed region.

Δm^2	$\sin^2(2\theta)_{BEST}$	90% C.L. $\sin^2(2\theta)$
1 eV^2	-0.14	0.34
10 eV^2	-1.9×10^{-3}	4.9×10^{-3}
26 eV^2	-3.7×10^{-4}	2.1×10^{-3}
50 eV^2	3.7×10^{-4}	2.8×10^{-3}
75 eV^2	1.1×10^{-6}	2.4×10^{-3}
100 eV^2	2.4×10^{-4}	3.0×10^{-3}
150 eV^2	4.0×10^{-4}	2.8×10^{-3}
200 eV^2	3.2×10^{-4}	2.6×10^{-3}
250 eV^2	5.8×10^{-4}	3.2×10^{-3}

Table 7.1: $\sin^2(2\theta)_{BEST}$ and 90% C.L. Limits for various Δm^2

an order of magnitude. Also, results from the SPY collaboration on the study of the pion to kaon ratios at different energies from 450 GeV protons on beryllium should be able to provide a useful comparison with the empirically derived neutrino spectrum used.

Bibliography

[1] Clowes, Dan, *Eightball*, Episode**9**, (Fantagraphics Books Inc., 1993).

[2] Cahn, Robert N. and Gerson Goldhaber, *The Experimental Foundations of Particle Physics* (New York, Cambridge University Press, 1991).

[3] Reines, F. and C.L. Cowan, Jr. "Free Antineutrino Absorbtion Cross Section. I. Measurement of the Free Antineutrino Absorbtion Cross Section by Protons," *Physical Review* **113** 273 (1959).

[4] Danby, G., et. al., "Observation of High–Energy Neutrino Reactions and the Existence of Two Kinds of Neutrinos," *Physical Review Letters* **9** 36 (1962).

[5] Perl, M. L. *et al.*, "Evidence for Anomalous Lepton Production in e^+e^- Annihilation." *Phys. Rev. Lett.*,**35**, 1489 (1975).

[6] Particle Data Group, *Phys. Rev. Lett.* **D34** (1996)

[7] Kesyer, B.,*Phys. Rev. D*, **24**,110 (1981)

[8] Bahcall, J.N. and Pinsonneault, M. H., *Rev. Mod. Phys.* **64**, 885 (1992).

[9] Langacker, P., *32nd International School of Subnuclear Physics*, Erice, 1994

[10] Wolfenstein, L.,*Phys. Rev.*, **D17** 2369 (1978)

[11] Mikheyev, S. P., Smirnov, A. Yu., *Nuovo Cimento* **C9** 17 (1986)

[12] Hirata, K.S. *et al.*,*Phys. Lett.* **B280**, 146 (1992)

[13] Becker-Szendy, R. *et al.*, *Phys. Rev.* **D46** 3720 (1992)

[14] Berger, Ch., *et al.*, *Z. Phys.*,**C66** 417 (1995)

[15] Aglietta, M. *et al.*, *Europhys. Lett* **8** 611 (1989)

[16] Goodman, M.C. *et al.*, *Nucl. Phys. B (Proc. Suppl.),* **B38**,337 (1995)

[17] Anselmann, P. *et al.*,*Nucl. Phys. B (Proc. Suppl),* **B38** 68 (1995)

[18] Abdurashitov, J.N.,*et al.*,*Nucl. Phys. B (Proc. Suppl),* **B38** 60 (1995)

[19] Cleveland, B.T.,*et al.*,*Nucl. Phys. B (Proc. Suppl)*,**B38** 47 (1995)

[20] Suzuki, Y.,*et al.*,*Nucl. Phys. B (Proc. Suppl)*,**B38** 54 (1995)

[21] Athanassopoulos, C. *et al.*, *Phys. Rev. Lett.*,**77**, 3082 (1996)

[22] Armbruster, B. *et al.*,*Proc. of Int. Europhysics Conf. on High Energy Phys. EPS-HEP97, Jerusalem*, Aug. 19-26, (1997)

[23] Altegoer, J. *et al.*, *The NOMAD Experiment at the CERN SPS*, CERN-PPE/97-059, (1997)

[24] Dignan, T. *et al.*, NOMAD by Numbers, NOMAD Memo, (1994)

[25] Astier, P. *et al.*, *NOMAD Reconstruction Software, Drift Chamber package version 7.1*, NOMAD Software Note, (1996)

[26] Bird I. G. , *Vertex finding and fitting package*, NOMAD internal note, (1996)

[27] GEANT *Detector Description and Simulator Package*, CERN Programming Library Long Writeup W5013

[28] Fasso, A., *et al.*, FLUKA92, in *Proc. of the Workshop on Simulating Accelerator Radiation Environments*, Santa Fe, NM, (1993)

[29] SPY Collaboration, G. Ambrosini *et al.*, CERN-SPSLC/96-01 (1996)

[30] Das, R. and Mishra, S. R., NOMAD Memo 97-038, (1997)

[31] Meyer, J. P., and A. Rubbia, *NOMAD Event Generator Off-Line Manual (Draft)* NOMAD Software Note, (1994)

[32] Ingleman, G., "LEPTO version 6.1—The Lund Monte Carlo for Deep Inelastic Lepton–Nucleon Scattering," *Physics at HERA* (proceedings), Hamburg, October 1991, v. 3., p. 1366.

[33] Altegoer, J., et. al., *NOMAD GEANT Offline Manual* Version 5.11, NOMAD Software Note, (1996)

[34] Fesefeldt, H.C., "*Simulation of hadronic showers*", PITHA report 85-02, RWTH Aachen

[35] Geiser, A. and Long, J., *Study of ν_μ-CC events and Comparison with NUBEAM, NEGLIB and GENOM* NOMAD Memo 97-005, (1997)

[36] Fazio, T., *et al.*, NOMAD Memo 95-041, (1995)

[37] Fazio, T., *et al.*,*TRD Simulation Package* NOMAD Software Note, (1993)

[38] Steffan, P., NOMAD Memo 97-013, (1997)

[39] Hanssgen, K. and Ranft, J.,"The Monte Carlo Code NUCRIN", *Computer Physics Communications* **39** (1986), 53

[40] Baker, S. and Cousins, R. D., *Nuclear Insturements and Measurements*,**221**, 437,(1984)

[41] Feldman, G. J. and Cousins, R. D., NOMAD Memo 97-047, (1997)

[42] Weber, F., NOMAD Memo 97-029, (1997)